Plant Archives
Journal home page: www.plantarchives.org
DOI Url: https://doi.org/10.51470/PLANTARCHIVES.2021.v21.no1.130

PHYTOPRODUCTION OF IRON NANOPARTICLES FOR METHYL ORANGE REMOVAL AND ITS OPTIMIZATION STUDIES

Yogita Sharma and Rachna Bhateria*

Department of Environmental Science, Maharshi Dayanand University, Rohtak, Haryana, India

* Email: bioremediationlab.mdu@gmail.com

(Date of Receiving-15-12-2020; Date of Acceptance28-03-2021)

ABSTRACT

In the present study, iron nanoparticles have been synthesized using the leaf extract of potential weed *Datura inoxia* to evaluate their feasibility for methyl orange removal. This method approves that the green synthesis method must be adopted for the more efficient and rapid synthesis of metal nanoparticles. A simple process of bio reduction has been involved, the leaf extract of *Datura inoxia* used as a precursor for reducing metal iron. The UV- visible spectral analyses for iron nanoparticles have shown a peak at 240 nm wavelength. Spherical shaped iron nanoparticles are formed as shown by transmission electron microscopy. Batch studies were investigated for optimization study of methyl orange removal on selected parameters i.e., pH (1-10), adsorbent dose (0.02-0.14g), initial dye concentration (5-100pm), contact time (15-120 minutes) and temperature (20-50°C). The result from the present study approves easy and fast dye removal of 98 % with kinetic data following a second order removal rate. The thermodynamics parameters supported the spontaneity with a negative value of ΔG i.e., -14.87 kJ mol^{-1} and exothermic (ΔH -7.094 kJ mol^{-1}) nature of the reaction. Thus, it can be concluded that the use of *Datura inoxia* for the phyto production of iron nanoparticles is efficient for various commercial applications in environment sector.

Keywords: Antioxidant activity; ABTS; *Bryophyllum pinnatum*; DPPH; Lectin; SDS-PAGE.

INTRODUCTION

Pure water is good for humans and their health and also essential feedstock used in many industries (Cao and Li 2014). Azo dyes are being used in the leather, textile, food, plastic, cosmetics, and paper and pharmacology industries for coloring purposes (Kim and Choi 2017). The effluent containing dyes are released into the water bodies, intensify its chemical oxygen demand (COD), biological oxygen demand (BOD) and suspended solids etc. In an investigation by Bhatia *et al* (2018) on textile effluent on 2 sites in Ludhiana, Punjab, recorded pH in the alkaline range (8.58-8.33) and suspended solids (143.5 ± 75.01 and 139.66 ± 71.87 mg L^{-1}) in autumn and lowest (86.50 + 15.10 mg/L) in the rainy season. Study also found out that the effluents were having values of BOD and COD ranged from 121–580 to 240–990 mg L^{-1}, respectively. These values are higher than the water quality standards provided by world health organization i.e., BOD - 30 mg $L^{-1}$and COD - 250 mg L^{-1}.

Also, it hinders the entry of light into the water; affect photosynthesis in aquatic plants, microbial growth, fish and other organisms' aquatic toxicity etc. The most important, it is also carcinogenic and mutagenic for human beings as well (Sajab *et al*., 2011). An azo (–N=N) group is present in azo dyes. According to the World Bank, estimation nearly 17–20% of water pollution contribution is related to dyeing industries and textile finishing (Kant 2011). In a survey by Ecological and Toxicological Association of Dyes and Organic Pigments Manufacturers (ETAD), out of 4000 dyes tested 90% had their LD50 values more than 2×103 mg kg^{-1}. However, the rate of toxicity was higher in tests done for azo, basic and direct dyes. About 15% (1000 tons) of non-biodegradable and toxic dyes are discharged into the water bodies through textile waste effluents annually (Ajmal *et al*., 2014). Production rate of dyes per annum is higher than 7×10^5 metric tons globally (Yao *et al*., 2016).Specific features that contribute to mutagenicity of azo dyes are related to differences in substitution sites, and the number and position of hydroxyl and sulpho-groups adjacent to the azo bond. Dyes are more toxic which have hydroxyl group at the ortho position in comparison to hydroxyl group at para position (Tauber *et al*., 2005). Precursor compounds used for manufacturing many azo dyes are known carcinogens, for e.g., naphthalene, benzidine and other aromatic compounds. Aromatic amines are released after cleavage of azo bonds by microflora containing azoreductase (Prasad and Aikat 2014). Moreover, in living creatures whenever azo dyes react with sweat, gastric juices and saliva aromatic amines are synthesized (Pielesz *et al*., 2002).High resistant of aromatic amines towards conventional wastewater treatment strategies makes them more persistent in the environment than dyes (Chen *et al.,* 2009). Also, water-soluble azo dyes get reduce into aromatic amines by the intestinal microflora in the gastrointestinal tract, which is reabsorbed and forms tumors. *N*, *N*-dimethyl-*p*-phenylenediamine (DMPD) (Figure 1) a mutagen produced from methyl

orange by intestinal anaerobes (Feng *et al*., 2012). Methyl orange (MO) is a toxic water-soluble azo dye which has use in laboratories, paper and textiles industries (Fan *et al.,* 2009). Discharge of MO through effluent from dye using industries into water bodies is causing many health hazards as MO is toxic, mutagenic and carcinogenic (Mathur *et al*., 2012). This has led to the use of several removal techniques for azo dyes from the environment. Various conventional and advanced treatment techniques have been used for treating dye-containing textile effluent like flocculation, adsorption (activated carbon sorption), UV-light degradation (Atul *et al*., 2012), fenton oxidation, membrane filtration, phytoremediation, bioremediation, photochemical, electrochemical oxidation (Ghaly *et al.,* 2014). Youssef *et al*., (2016) has reported the oxidation of MO using a Fenton reaction and achieved a removal of 97.8%. The use of cork powder for MO removal by Kriya and Benlahbib (2015) proved to be an improved study with good adsorption capacity of cork for MO 16.66 mg g^{-1} at pH 2, 298 K or 25 ^{o} C and 5.00 g cork dosage, particle size of d<0.08 mm and contact time of 240 minutes in optimal conditions. However, these removal methods have some limitations like photochemical degradation forms toxic byproducts, flocculation method produce sludge while electrochemical oxidation is too expensive (Raman and Kanmani 2016).

Currently, a novel field has been fabricated called nanobiotechnology by converging nanometer scale technologies with biological technologies. This new field mainly focuses on creating, manipulating and using materials at the nanometre scale for highly developed biotechnology (Goodsell 2004). Moreover, nanobiotechnology is based on the principles of biology with chemical and physical methods to create nanoparticles (NPs) of unambiguous properties (Kathiresan *et al*., 2009). However, "A nanoparticle can be defined as any intentionally produced particle that has a characteristic dimension from 1 to 100 nm and has properties that are not shared by non-nano scale particles with the same chemical composition" (de Medecine 2009). The smaller size is associated with intensification in number of atoms on the surface and demarcates the groups of NPs (Lin *et al.,* 2005). The most important property of (Daniel and Astruc 2004). NPs are to act as a catalyst or to catalyze the reactions which are impossible to achieve 9. Kaur *et al*., (2013) evaluated the potential of zinc oxide nanoparticles for MO removal byphotocatalytic degradation and attained a complete degradation in 80 minutes. Recently, metal NPs synthesis from leaf extract of different plants is an alternative to other synthesis methods and promises inexpensive and non- toxic reduction process (Machado *et al*., 2013). Hence, the green synthesis approach for NPs fabrication by means of phytochemicals extracted from weeds that act as reducing agents is striking one. These phytoconstituents can transform metal ions into metal NPs (Mittal *et al*., 2013) by the process of reduction. Even, there is no need for ligand exchange before biological applications as they act as capping agent as well (Sebastian *et al.,* 2018). Metal NPs of several shapes and size are being formed by means of reduction of metals in the presence of phytochemicals (Pattanayak and Nayak 2013a). Mondal (2015) reported the biosynthesis of silver nanoparticles using aqueous shoot extract of *Parthenium hysterophorus* at room temperature along with using it for degradation of MO dye.

Nowadays, iron nanomaterials due to their versatile properties and high catalytic activities and the higher intrinsic reactivity of its surface sites have received great attention from researchers in different fields such as medical uses (Silva *et al*., 2016), degradation of environmental organic contaminants (Wang *et al.,* 2015), catalysis (Walker and Zaleski 2016), magnetic storage media (Yu *et al*., 2016), magnetic field-assisted separations (Massoud and Mahmoud 2017). Iron oxide nanoparticles as dye removing materials are used for maintaining a healthy environment (Ebrahiminezhad *et al.,* 2018). Green-synthesized Fe NPs has been examined for dye degradation and because of the easy availability of plants in nature; it makes them more applicable (Saif *et al*., 2016). Ebrahiminezhad *et al*., (2018) used *Cupressus sempervirens* for synthesis of iron nanoclusters of mean size 19nm. The potential of green synthesized iron nanoclusters was analysed for MO removal.

The present study aimed to prepare a phytochemical extract from the leaves of potential weed of Rohtak i.e. *Datura inoxia* to reduce iron salt precursors into FeNPs. *Datura inoxia* (*D. inoxia*) is a potential weed and a well-known Indian medicinal plant belonging to the family *Solanaceae*. Many different bioactive molecules found within its extract are responsible for the reduction of the metal iron to Fe NPs. Furthermore, the use of Fe NPs for methyl orange (MO) removal from textile wastewater indicates that they have good phytochemical content which leads to new interactions amid dye species and metal NPs. A methodical study of the influence of pH, adsorbent dose, contact time, initial dye concentration and temperature on MO dye uptake by Fe NPs was explored in this study. However, to the best of our knowledge, Fe NPs synthesized using *D. inoxia* species have not been explored towards the removal of MO removal so far.

MATERIALS AND METHOD

Chemicals Used

Ferric chloride (anhydrous) was purchased from Ranbaxy Fine Chemicals Ltd. Double distilled water was used for extract preparation as well as synthesis process. Methyl orange [4-dimethylaminoazobenzene-4-sulfonic acid, sodium saltHazardous Substances Data Bank Number: 4322] is an orange powder (Figure 2) (NTP 1992). In double distilled water, stock solution of MO (1000 mg L^{-1}) was prepared.

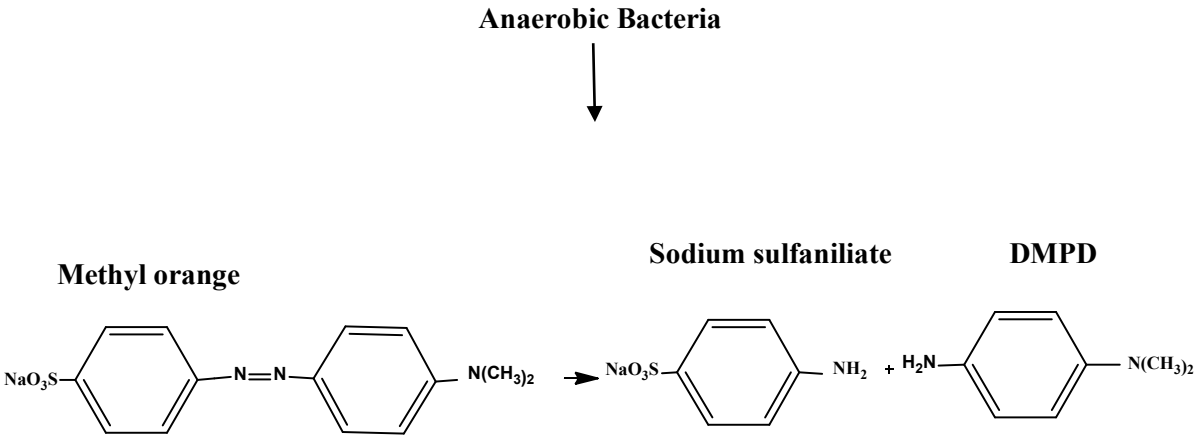

Figure 1 Azo reduction of methyl orange

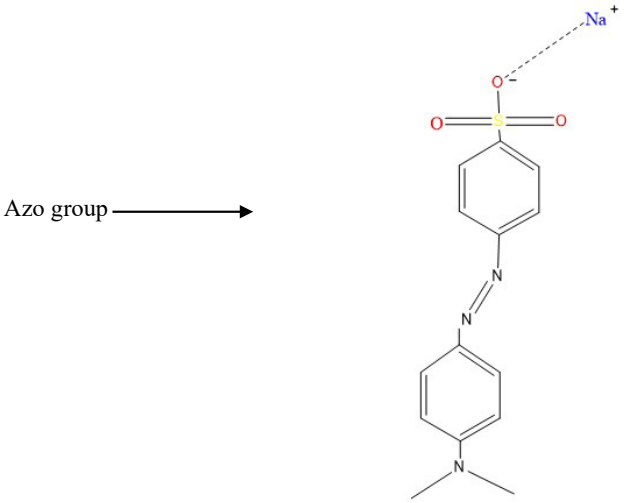

Figure 2 Structure of Methyl Orange

Table 1. Linear forms of the adsorption isothermsmodels

Isotherms	Linear	Plots
Langmuir	1/qe=(1/b*qe) * (1/Ce) + (1/qm)	
Freundlich	ln (qe) =ln K_F +(1/n) * ln (Ce)	
Temkin	RT /b ln AT	ln Ce *vs* qe

Table 2. Parameters for Langmuir Isotherms

TYPES	q_m (mg g^{-1}) (Maximum adsorption layer capacity)	b (mg L^{-1}) Energy change in adsorption	R^2 Coefficient of Determination	R_L (Dimensionless constant)
Langmuir	81.967	8	0.99	0.145

Weed Collection

The potential weed *D. inoxia* is available throughout the year. The leaves of this weed were collected from Maharshi Dayanand University (M.D.U.), Campus, Rohtak and nearby villages within the Rohtak city. The GPS points taken of these sites are shown in the map (Figure 3), Rohtak with Coordinates 28.8909°N 76.5796°E.

Leaf Extract Preparation

Fresh leaves were collected of *D. inoxia* for the extract preparation. For removal of any dirt and organic contaminants, the leaves were cleaned with running tap water and kept in a sieve for some time to remove extra water (protecting the leaves from degradation), chopped into small pieces and then shade dried. To make the powder, leaves were oven dried at 60° C. Addition of 5% (w/v) powder of leaves with double distilled water is a much-generalized ratio for the preparation of leaf extracts (Ebrahiminezhad *et al*., 2017). For this, 5 g dried leaves were boiled in 100 ml double distilled water for 15 minutes on a hot plate. The prepared extract was left for an hour at room temperature for cooling. The extract prepared was centrifuged at 2000 rpm for 5 minutes (at room temperature) to remove leaf micro particles (Beheshtkhoo *et al*., 2018).

GC-MS Analysis

The carrier gas was helium (99.999%), used at a flow rate of 1.2 ml min^{-1} with split mode (10:1). 1 µl of methanol sample was injected into column at 250°C injector

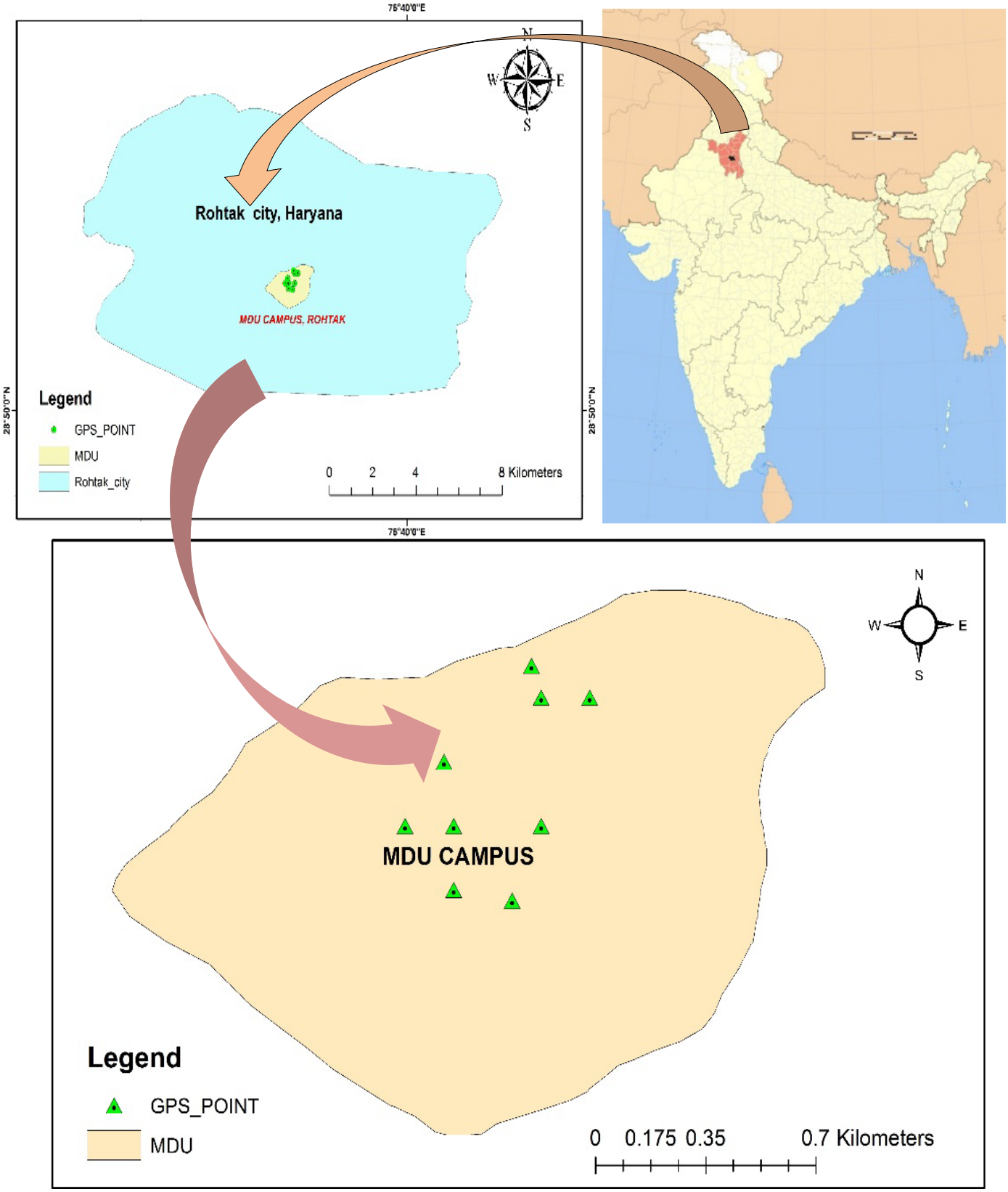

Figure 3 Map showing weed collection area

temperature. The initial temperature of the oven was kept at 150°C and then increased at the rate of 10° C min^{-1} up to 200°C. Then it was raised at a rate of 5 deg C/min^{-1} up to 220° C with a hold time of 19 minutes. The temperature of ion sources was maintained at 210° C. Total running time of a sample was 28 minutes. The identification of compounds in the sample was performed by comparing the mass spectra of compounds in the sample with NIST (National Institute of Standards and Technology) library.

Green synthesis of Iron Nanoparticles

Ferric chloride ($FeCl_3$) (anhydrous) (Ranbaxy Fine Chemicals Ltd. CAS: [7705-08-0]) was used for metal ion solution. FeNPs formation was screened by mixing of ferric chloride solution (0.10 M) with the leaf extract (2:3) by continuous stirring for half an hour with further addition of NaOH. The solution turned into a black color

solution indicating the formation of FeNPs. The FeNPs were separated from the solution through centrifugation at 15000 rpm. The pellet of FeNPs obtained was washed three times with double distilled water and dried (Shahwan *et al*.,2011).

Characterization

D. inoxia leaf extract was analyzed by Gas chromatography-Mass spectrometry (GC-MS) (Thermo Fisher) to detect the presence of phytoconstituents. Spectroscopic analysis was performed by UV-vis spectrophotometer (LabIndia, UV) and the wavelength range was set from 200 to 600 nm. For size determination of FeNPs, these were subjected to transmission electron microscopy (TEM) (Talos 200kv Cryo TEM). The crystallinity of the sample was investigated with X-ray diffraction (XRD) analysis (Rigaku Ultima IV, Ri).

Batch adsorption studies

Batch experiments were performed for investigating the effects of parameters *i.e.,* pH, adsorbent dose, initial dye concentration, temperature and contact time on dye adsorption. Batch adsorption studies were performed by suspending FeNPs (0.02−0.14 g L^{-1}) in MO working solutions of different initial dye concentrations (5−100 ppm) of different pH values (1-10). The solutions were rotated at 150 rpm at constant temperature (298 K). The desired pH of the solutions was set up by 0.01 N HCl and 0.01N NaOH. The solutions were filtered using Whatman filter paper No 1 for minimizing the effects of suspended particles in solution. The concentration of MO in the supernatant was estimated by UV/visible spectrophotometer at 464 nm (MO maximum wavelength) using a calibration curve. The results presented here are the mean of triplicate determination.

Estimation of removal efficiency

The percentage removal (% R) of the dye solution and amount of dye adsorbed (qe, mg g^{-1}) on the adsorbent were calculated by equations (Eq) (1) and (2) respectively:

$$R(\%) = \left(\frac{C_o - C_e}{C_o}\right) * 100 \quad \text{Eq. (1)}$$

$$qe = \frac{(C_o - C_e) * V}{W} \quad \text{Eq. (2)}$$

The adsorption capacity (qe) is defined as "the amount of adsorbed material per mass of adsorbent" (do Socorro *et al.,* 2016). Where qe (mg MO g^{-1} adsorbent) is "the amount of dye adsorbed on per gram adsorbent at the time of equilibrium", V (L) is the volume of solution and C_o and C_e (mg L^{-1}) are the initial and at equilibrium dye concentrations respectively, W denotes dry weight of adsorbent (g).

RESULTS AND DISCUSSION

GC-MS Analysis

The GC-MS analyzed that *D. inoxia* leaf extract was rich in phyto constituents like phenols and alcohols which were responsible for the reduction of FeNPs (Figure 4). The peak at 8.33 (Retention time, RT) is of 2-methoxy-4-vinylphenol that is a plant metabolite, a member of the class of phenols**.** The peak at 14.68 (RT) shows *D. inoxia* leaves are rich in phytol or 3, 7, 11, 15-tetramethyl-2-Hexadecen-1-ol. Phytol is acyclic diterpene alcohol while compound n-hexadecanoic acid also found with RT 26.26. Hexadecanoic acid is a potential antioxidant as well (Sundararajan *et al*., 2017). On the parallel lines, Bagewadi *et al*., (2019) also analyzed phytol (RT-14.78) and hexadecanoic acid (RT 5.094) in *D. inoxia* leaf extract.

UV-visible spectral analysis

After adding ferric chloride solution to *D. inoxia* leaf extract, the color changes to black, confirms Fe NPs fabrication. UV- visible spectroscopic analysis was carried out and a sharp peak obtained at 240 nm for FeNPs whereas at 290 nm for leaf extract (Figure 5). Likewise, Pattanayak and Nayak (2013b) monitored the UV-vis peaks between 216-265 nm wavelengths for bio reduction of Fe^{3+} which were similar to the UV-visible peak of metal iron.

FT-IR Spectroscopy

The FT-IR analysis was carried out to know the presence of functional groups in *D. inoxia* extract which played the role of reducing, capping and stabilizing agents in FeNPs synthesis (figure 6a). FT-IR spectra of FeNPs synthesized from *D inoxia* extract is carried out as well (figure 6b). Broad peak at 3342 and 3416 cm^{-1} refers to O-H stretch of H bonding in alcohols and phenols while the peaks at 2975 cm^{-1} and 2897 cm^{-1}, 2924 cm^{-1} and 2855 cm^{-1} (Figure 6a, b) can be ascribed to the C-H stretching vibration of a methylene group. 1647 cm^{-1} peak is slightly shifted to 1631 cm^{-1} as it shows the presence of C=C stretching. The peak at 1044 cm^{-1} representing C-O stretching vibration of primary alcohols. This peak is not well formed; it may conclude that primary alcohols have been used in the synthesis of FeNPs. This indicates the putative role of alcohols and phenols played significant role in FeNPs fabrication.

Transmission Electron Microscopy

The size as well as the morphology of green synthesized FeNPs was assessed with the help of TEM. TEM micrograph of the FeNPs synthesized by *D. inoxia* leaf extract is shown in Figure 7 (a). A single drop of FeNPs was positioned on a copper grid coated with carbon and dried (at room temperature) before processed for TEM.TEM images showed that the majority of FeNPs were spherical

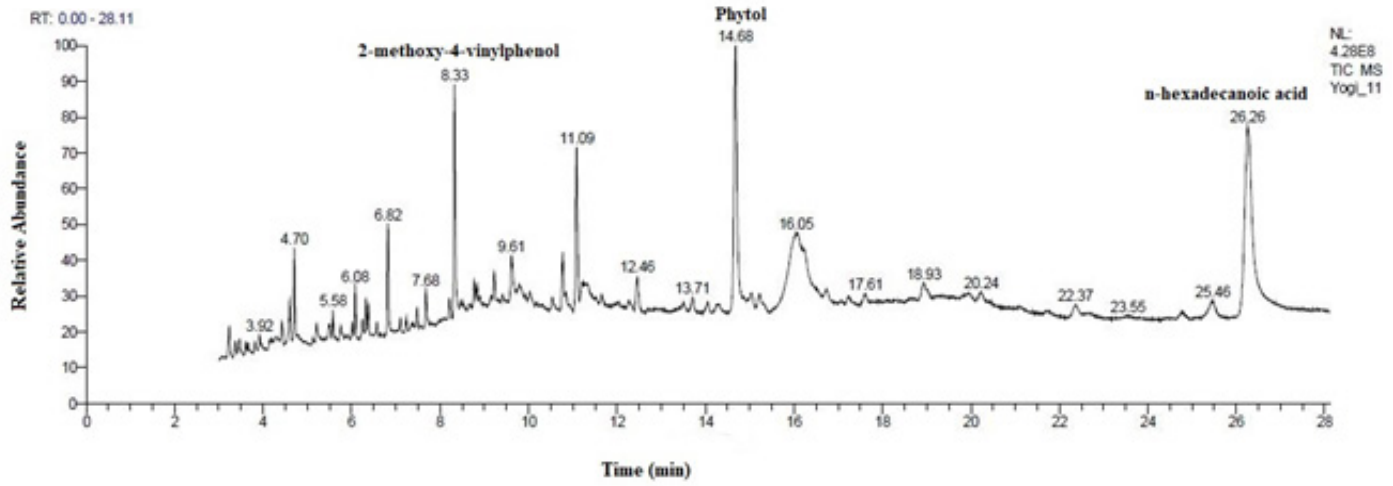

Figure 4 GC MS chromatogram of methanolic leaf extract of Datura *inoxia*

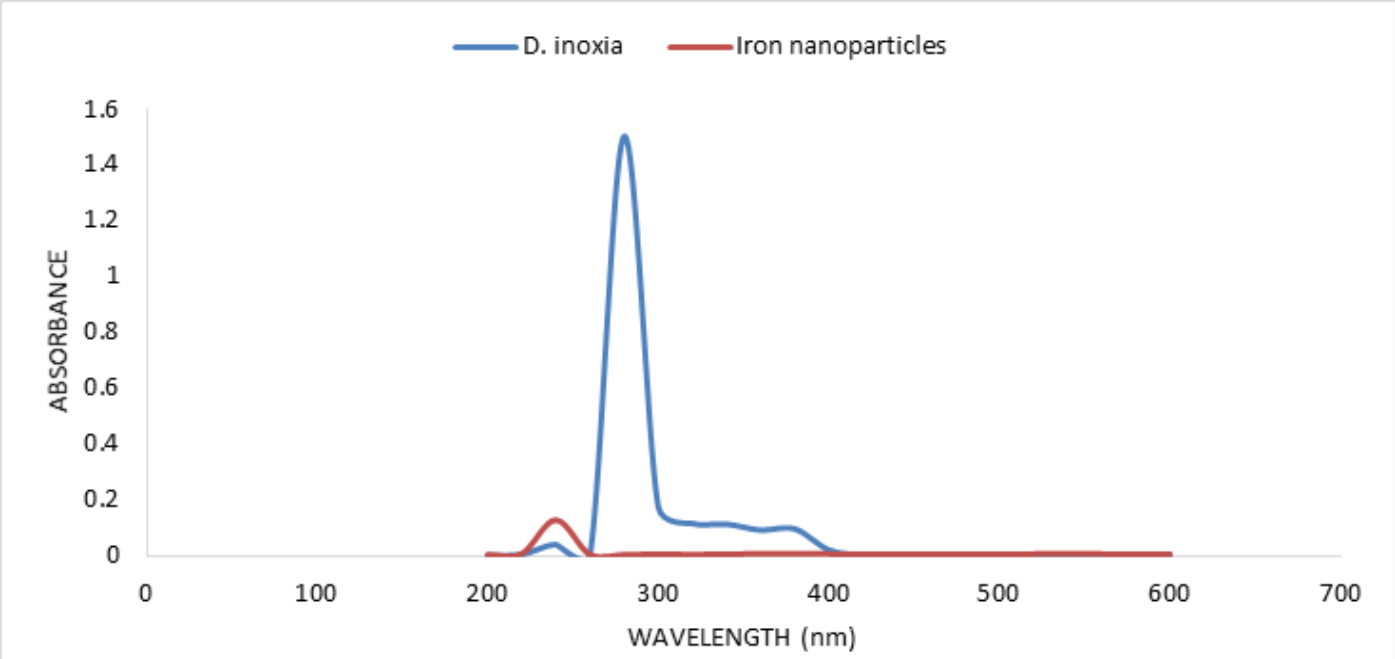

Figure 5 UV-vis spectral analyses of FeNPs synthesized using Datura *inoxia* leaf extract

shaped in a chain like structures under nanoparticle size range (1-100nm). A fine layer of biomatrix surrounding the FeNPs confirms the presence of plant biomolecules present in *D. inoxia* leaf extract which reduced Fe ions to FeNPs. Nanoparticles subjected to transmission electron microscope were coupled to energy dispersive X-ray spectroscopy (EDX).

The EDX of FeNPs was done for determining the chemical composition (Figure 8). An EDX spectrum shows intense peaks of Fe, Oxygen, carbon and chlorine as well. Atomic percentages as given by EDX: Fe (7.25%), O (14.85%), C (65.29%) and Cl (9.32%). Oxygen is also present suggesting surface oxidation of the FeNPs (Njagi *et al.,* 2011). Chorine might be originated from $FeCl_3$. Presence of copper and carbon peak is due to a carbon-coated copper grid used in TEM analysis. Selected area electron diffraction (SAED) pattern confirms the FeNPs are amorphous in nature (Figure 7 b).

Field Emission Scanning Electron Microscopy (FE-SEM)

FE-SEM was done for morphological analysis the of the fabricated FeNPs. Figure 9 shows the granular and spherically shaped FeNPs with mean size 14 nm (mean: 14 nm). In addition, the capping of plant biomolecules was vital for avoiding the FeNPs aggregation which enhanced their stability as well (Ali *et al*., 2018). To study the morphology of the synthesized FeNPs Freyria *et al*., (2017) has done the FE-SEM and analyzed that spherical shaped FeNPs were formed with size 110nm.

X-Ray Diffraction

Figure 10 illustrates the XRD pattern of Fe NPs; the scanning range used for the sample analysis was $10° \leq 2\theta \geq 80°$. The characteristic peaks at $2\theta = 32°$ corresponded to iron hydroxides while $2\theta = 45°$ shows the formation of an

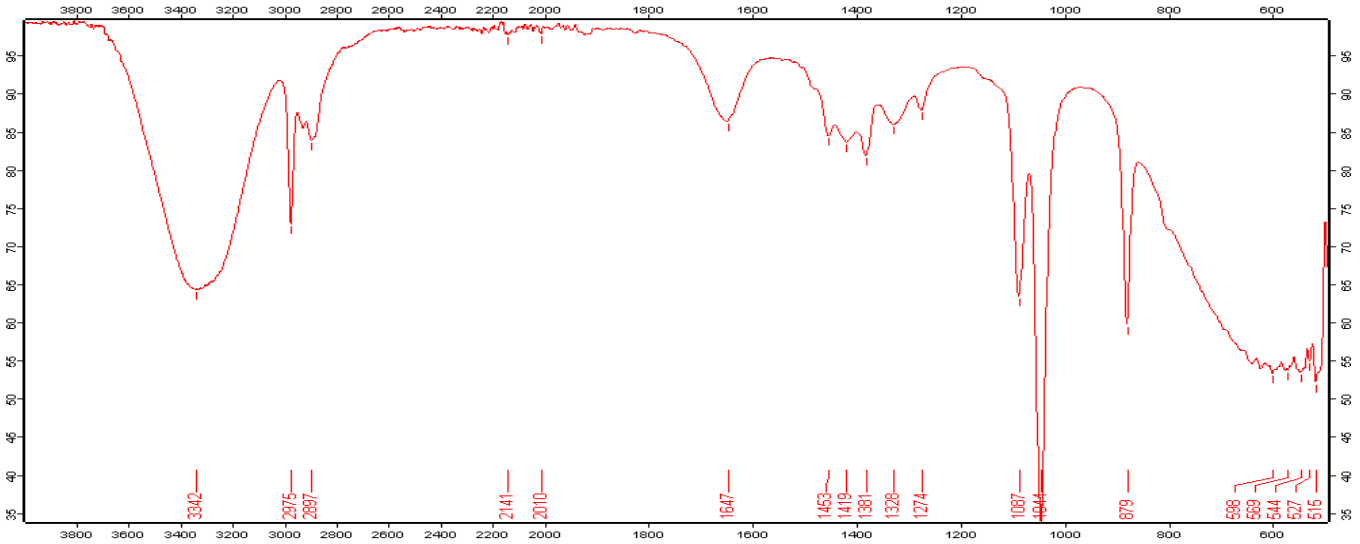

(a)

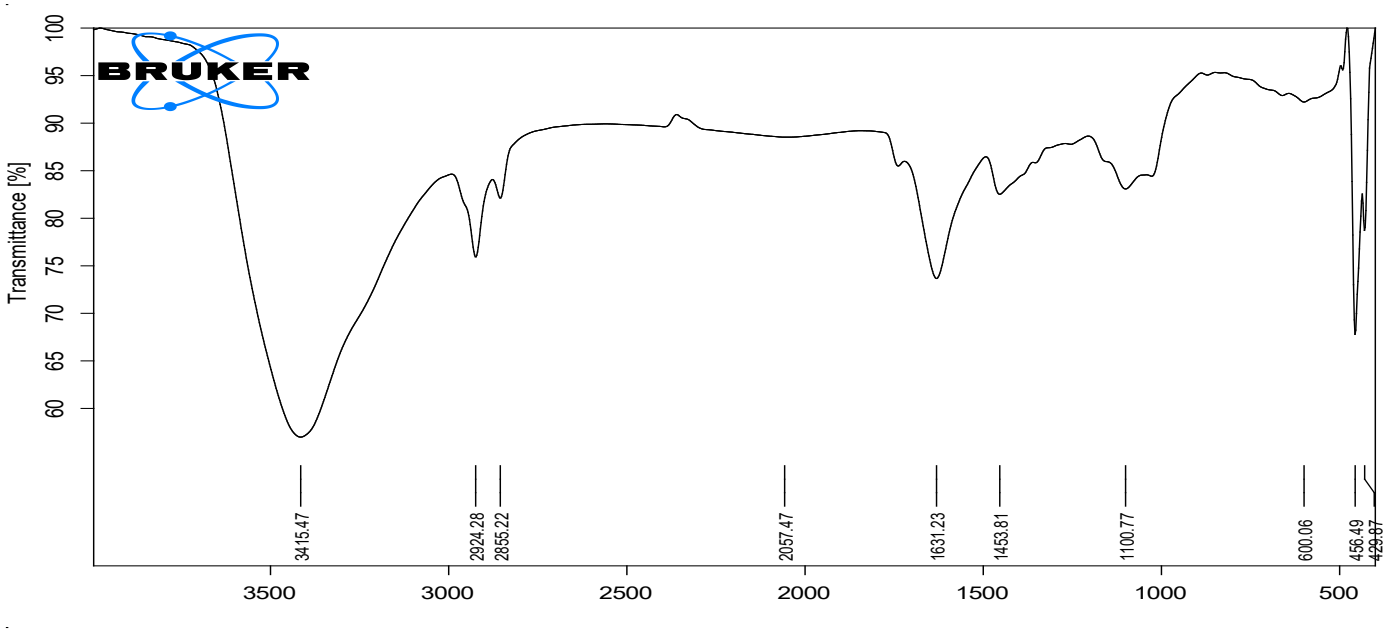

(b)

Figure 6 FT-IR spectra of (a) D. *inoxia* leaf extract (b) Iron Nanoparticles

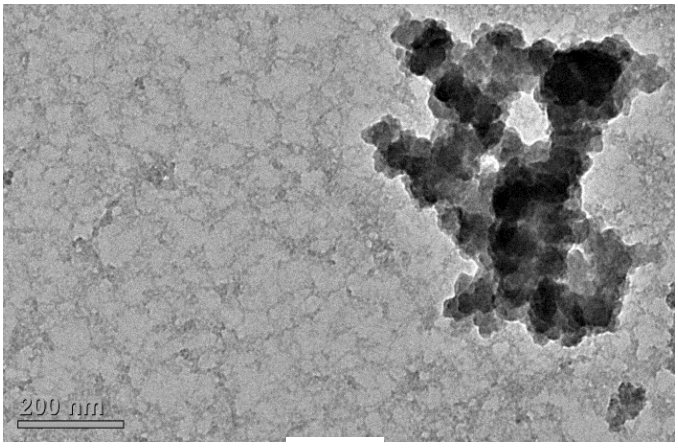

(a)

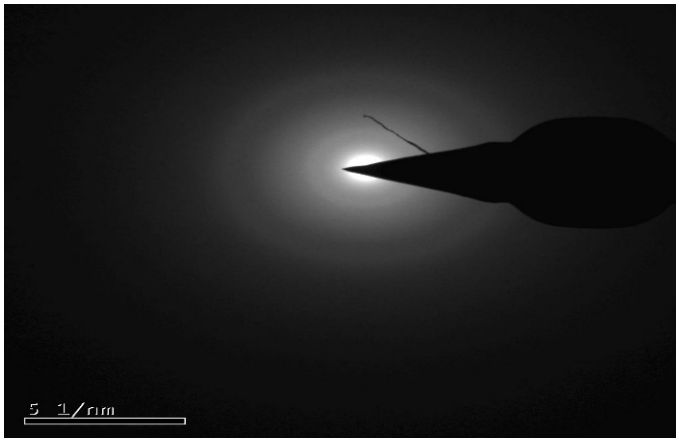

(b)

Figure 7 Transmission electron microscopy image of (a) FeNPs and (b) SAED pattern

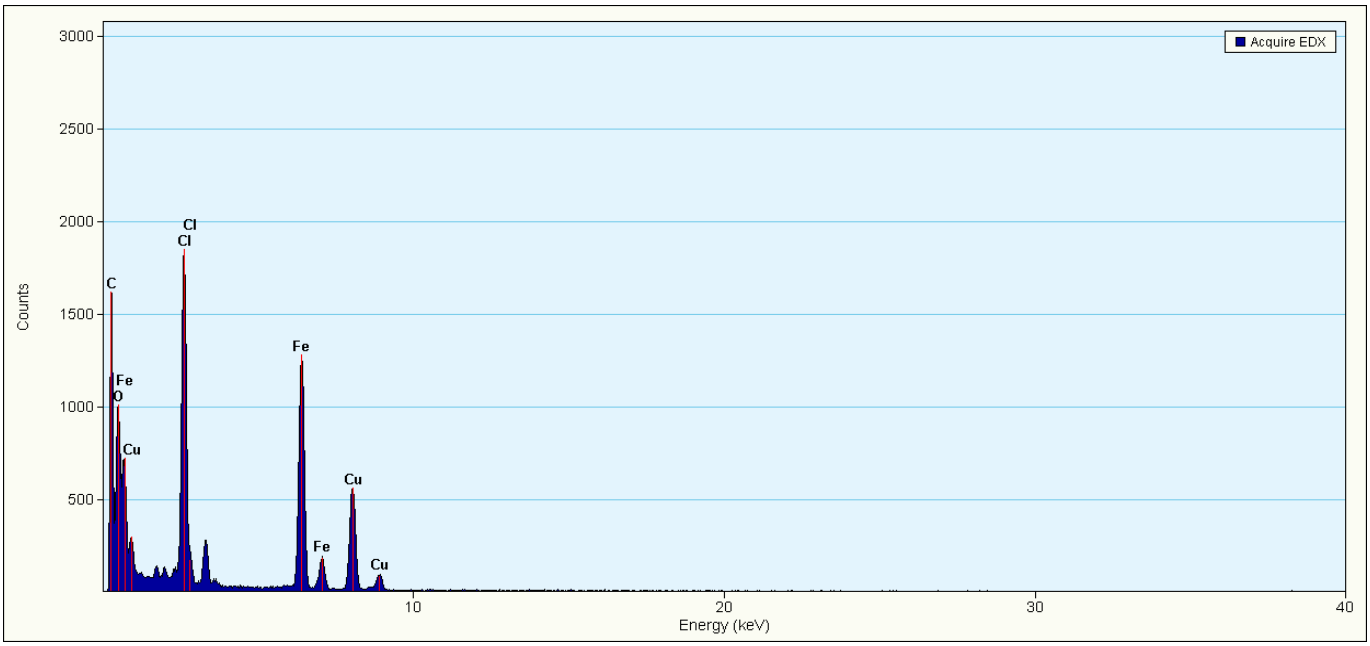

Figure 8 Energy Dispersive X-ray Spectroscopy

Isotherms	**Model Parameters**	**Values**
Freundlich	1/n	1.78
	N	0.558
	ln K_F	2.11
	K_F	8.32
	R^2	0.98
Temkin	B_T	478
	Ln A_T	1.85
	A_T	6.38
	R^2	0.99

Table 3. Linear forms of Freundlich and Temkin isotherm models

Kinetic models	**Model parameters**	
Pseudo I order	q_{eexp} (mg L^{-1})	0.3
	q_{ecal} (mg L^{-1})	1.765
	k_1 (min^{-1})	1.277
	R^2	0.98
Pseudo II order	qe_{cal} (mg L^{-1})	0.35
	k_2 (min^{-1})	0.003
	R^2	0.99

Table 4. Kinetic Adsorption Parameters

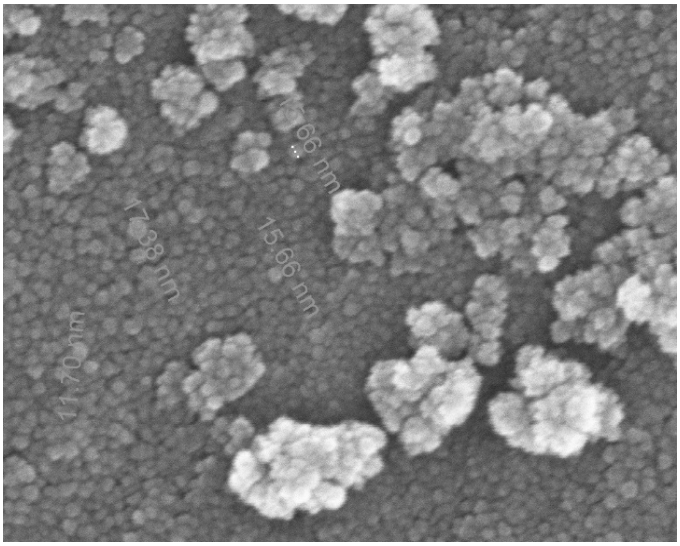

Figure 9 Field Emission Scanning electron microscopy image of FeNPs

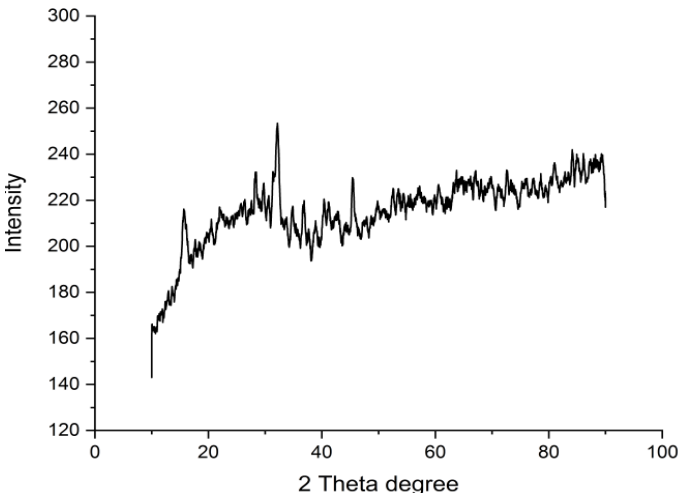

Figure 8 Energy Dispersive X-ray Spectroscopy

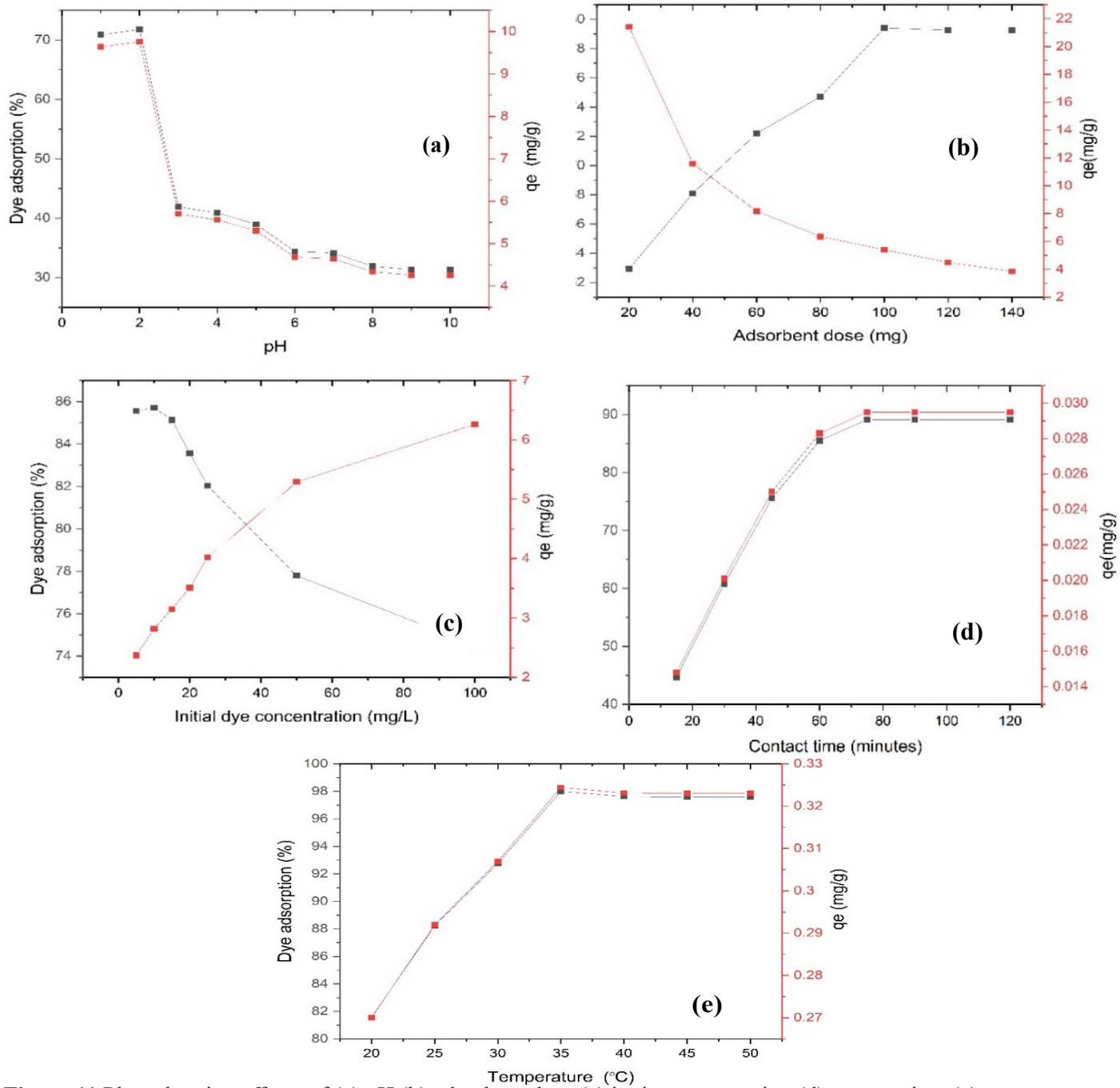

Figure 11 Plots showing effects of (a) pH (b) adsorbent dose (c) ionic concentration (d) contact time (e) temperature on methyl orange removal using Fe NPs

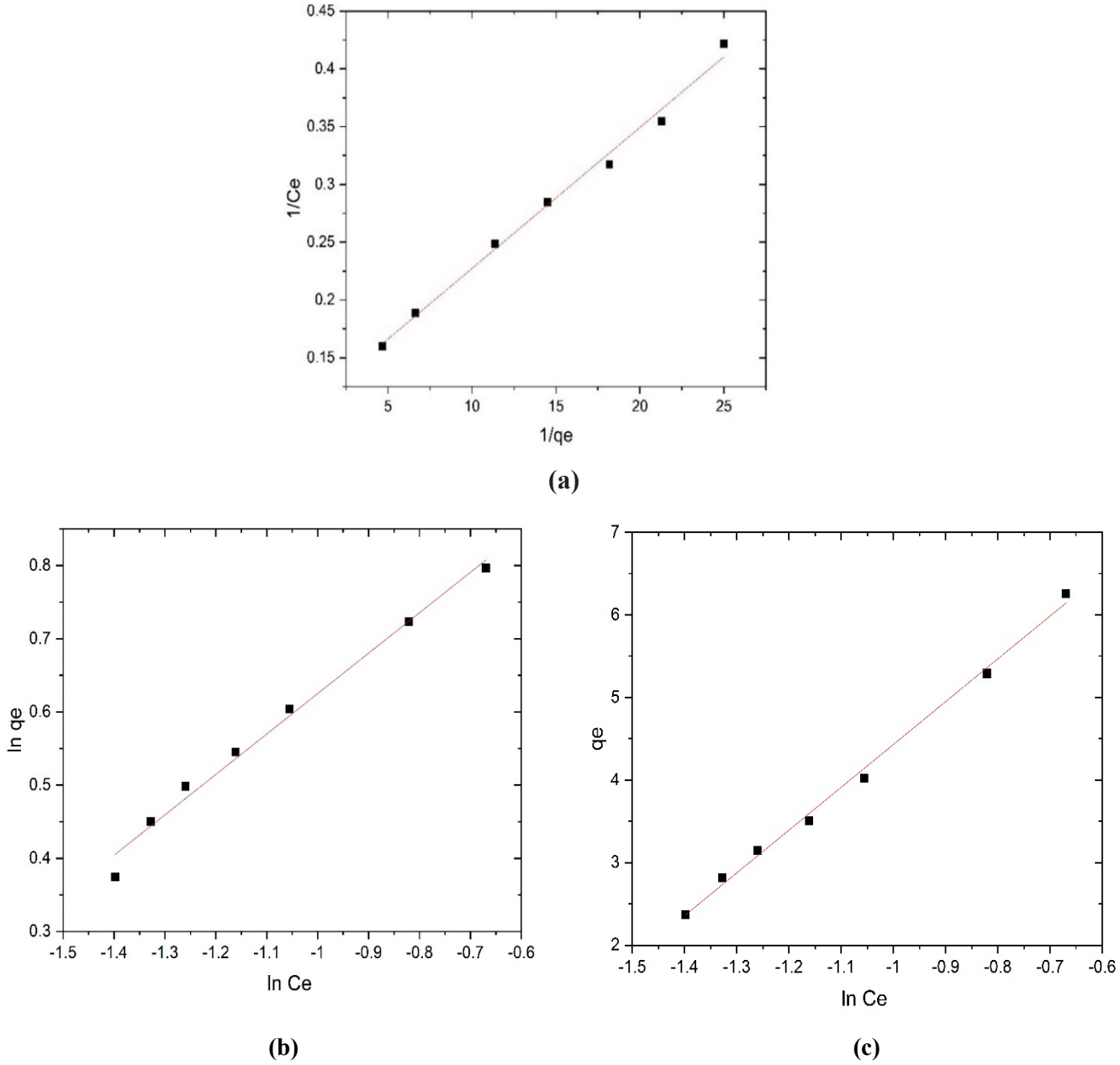

Figure 12 Plots of (a) Langmuir (b) Freundlich and (c) Temkin Isotherms

Table 5. Thermodynamic adsorption specifications

ΔH (kJ mol^{-1})	ΔS (kJ mol^{-1})	ΔG (kJ mol^{-1})			
		298	308	318	328
-7.094	0.026	-14.876	-15.1379	-15.3991	-15.6602

amorphous Fe phase (Kim and Choi 2017) which is ably supported by SAED pattern too. Kim and Choi (2017) also analyzed during XRD studies that a broad peak at 2θ = 45° depicts the iron is in amorphous phase. Also, Kheshtzar *et al*., (2019) investigated in his optimization studies for fabricating green synthesized iron nanoparticles that FeNPs were amorphous but not crystalline in nature.

Batch Studies for Dye removal

Influence of pH

Solution pH takes the important part in the adsorption of the dye MO by Fe NPs as it affects the aqueous chemistry in addition to surface binding-sites (OF adsorbent). At pH 2, the solution of MO achieved maximum decolonization efficiency of 72% within 60 minutes of reaction time. But on increasing the pH to 7 the dye removal decreases to 5% only and becomes constant for a further increase in pH up to 10 (Figure 11 a). At lower pH, iron surface becomes positively charged (Li *et al*., 2006) while MO (an anionic dye) molecules become negatively charged. Hence,

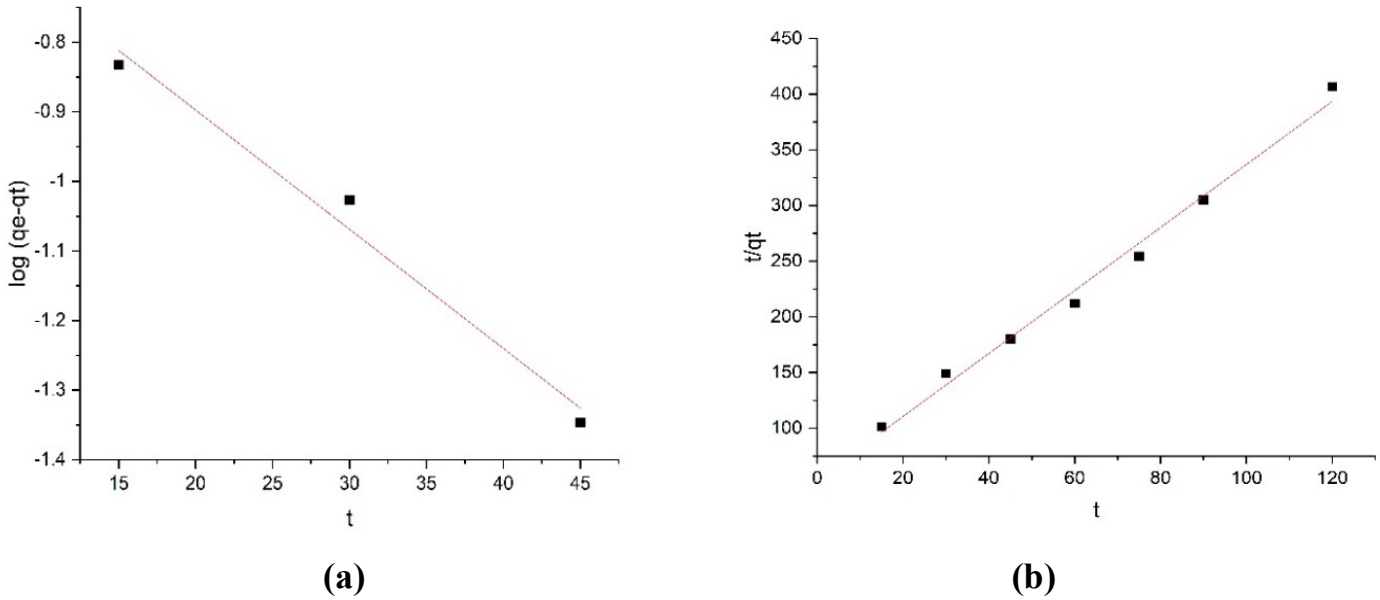

Figure 13. (a) Pseudo I order (b) Pseudo II order plots for MO removal

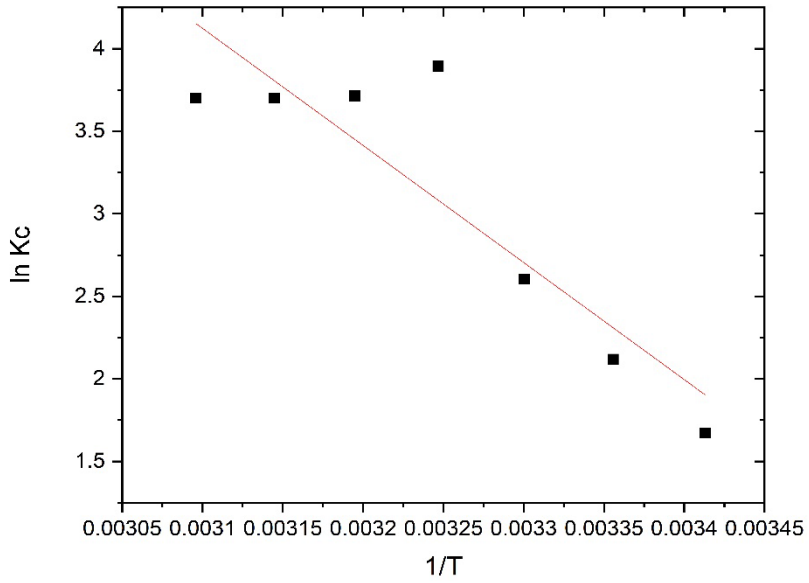

Figure 14. Arrhenius plot showing relationship between ln Kc versus 1/T for the MO removal using FeNPs

making favorable for the process of dye adsorption onto the surface of adsorbent (FeNPs). Conversely, when solution pH is alkaline, the Fe exterior loaded with negative charge (alkaline pH causes the corrosion products to cover the Fe^{o} surface (Fan *et al.,* 2009). This result suggests that acidic pH is favorable for MO removal, while reaction in alkaline conditions may retard. The study done by Debnath *et al*., (2016) also proves that the removal of MO using α-Fe_2O_3 NPs favors acidic medium.

Influence of Adsorbent dose

With other parameters kept constant a dosage range was selected. In figure 11(b) with an increase in FeNPs dosage qe (adsorption capacity, mg g^{-1}) value decreases, it is because of increase in surface area while keeping the adsorbate concentration constant (Saha *et al.,* 2011). During the reaction as more FeNPs are loaded, results in increase in surface area *i.e.* active and adsorptive sites. Hence, dye removal increases with increase in FeNPs loading within the same reaction time. Within a time of 60 minutes reaction reaches at equilibrium, efficiency of dye removal was 62%, 68%,72%,74% and 79.41 % respectively for the dosage 0.02, 0.04, 0.06, 0.08 and 0.1g.

Influence of ionic concentration

Figure 11 (c) depicts the effect of ionic concentration on MO removal using FeNPs in aqueous solution. An increase in dye concentration (5-100 mg L^{-1}) results in increase in MO amount adsorbed per unit mass of FeNPs *i.e.,* qe (2.23 to 6.26 mg g^{-1}). More dye molecules transfer towards adsorbent surface with an increase in dye concentration (5-100 mg L^{-1}). A concentration gradient creates at higher concentration between MO molecules in aqueous solution and MO on FeNPs surface. This concentration gradient is the driving force for mass transfer during adsorption process (Luo *et al.,* 2010). Though, the percentage removal decreases (85.55%-74.52%).

Influence of contact time

One of the significant design parameters is the contact time that affects the efficiency of adsorption process between adsorbate (MO) and adsorbent (FeNPs). Keeping the parameters pH, adsorbent dose as well as initial ion concentration constant (putting their optimum values) the variation in contact time was investigated for the performance of FeNPs for MO removal. Figure 11 (d) shows dye adsorption starts within 15 minutes after mixing FeNPs in MO containing solution and attained maximum removal capacity in 75 minutes.

Influence of temperature

Habitually, a chemical reaction shows delicate behavior towards temperature changes, which helps in understanding the mechanism of reaction (Liou *et al.,* 2005). The temperature effect on MO removal was investigated with an initial 10 mg L^{-1} MO concentration and 0.1 g FeNPs at original pH 2 for 75 minutes. In a temperature range of 20–50 °C experiments were conducted. Figure 11 (e) shows at low temperatures incomplete MO removal was recorded. The removal efficiency increased from 81 % to 98 % due to increase in temperature from 20 to 35°C. Higher temperatures shown to shorten the time needed for MO removal.

Adsorption Isotherm

The adsorption isotherms signify designing the adsorption mechanism and also characterize the adsorbent (Erdem *et al*., 2005). To design and optimize the process of adsorption it is necessary to develop an appropriate isotherm model. To evaluate the adsorption of any compound at equilibrium some isotherm models have been developed *e.g.,* Langmuir, Freundlich, Temkin, Dubinin–Radushkevich, Redlich–Peterson and Sips etc (Dabrowski 2001). Subsequently, Langmuir, Freundlich and Temkin are generally used for investigating the adsorption isotherm. In this experimental work, results were applied with these 3 adsorption isotherm models in addition isotherm plots were created based on experimental equilibrium data attained. Adsorption isotherm is stated as "the amount of adsorbate taken up per gram of adsorbent (qe mg g^{-1}) to the equilibrium solution concentration (Ce mg L^{-1}) at a fixed temperature". Constants of these adsorption models offer substantial parameters for envisaging adsorption potential.

Langmuir Isotherm

Langmuir model assumes that "the uptake of adsorbate molecules occurs on a homogenous surface with a finite number of adsorption sites" (Deng *et al.,* 2009). A site stops further adsorption forming amonolayer and reaches at saturation point through achieving maximum adsorption of the surface (Javadian and Taghavi 2014). Langmuir adsorption isotherm linear equation is shown in Table 1.

Where Ce denotes adsorbate concentration at equilibrium (mg L^{-1}) whereas q_m (q_{max}) conclude the maximum adsorption capacity (mg g^{-1}) while b denoted for Langmuir constant (L mg^{-1}) and signifies "the energy of adsorption process". Slopes and intercepts values obtained by plotting the Langmuir isotherm graph was used to calculate q_m and b (Figure 12 a). MO removal using green synthesized FeNPs fits to Langmuir adsorption isotherm model. R_L *i.e.* separation factor, is a significant component of Langmuir adsorption isotherm. R_L is a dimensionless constant and can be expressed as:

$$R_L = \frac{1}{1} + bCo \qquad \text{(Eq.3)}$$

Equation 3 signifies the adsorption behavior *i.e.,* for favorable adsorption, when value of R_L is within the range $0 < R_L < 1$ whereas $R_L > 1$ and $R_L = 1$ for unfavorable and linear adsorption respectively (Weber and Chakravorti 1974). R_L values calculated were within the range *i.e.,*0.142−0.933 (Table 2). As the R_L values are below 1 so it predicts the adsorption to be favorable for the present study for the under the applied experimental conditions.

Freundlich Isotherm

The Freundlich isotherm a primeval adsorption isotherm model, is suitable to apply for heterogeneous surface describes "relationship between the non-ideal and reversible adsorption" (Ayawei *et al.,* 2015). It is established on multilayer adsorption hypothesis which takes place on heterogeneous surfaces comprising non-uniform sites with dissimilar energy distribution. It is given by the linear equation (Hu *et al.,* 2010):

$$\log qe = \log K_F + \frac{1}{n} \log Ce \qquad \text{(Eq. 4)}$$

wheren and K_F are the Freundlich constants, here n is the heterogeneity factor and is associated with adsorption intensity whereas K_F to adsorption capacity (mg g^{-1}). n value indicates the adsorption process is favorable or not, the values below 1 shows favorable adsorption. By plotting the graph between log qe and log Ce, the values for K_F and n can be obtained (figure 12 b) and are summarized in table 1.

Temkin Isotherm

The Temkin adsorption isotherm model adopts the phenomenon that "the adsorption energy decreases linearly with the surface coverage due to adsorbent–adsorbate interactions". The linear equation for Temkin isotherm is as follows (Kiran and Kaushik 2008).

$$q_e = \frac{RT}{B_T} \ln A_T + \frac{RT}{B_T} \ln Ce \qquad \text{(Eq. 5)}$$

Where B_T denotes Temkin constant which is associated with adsorption heat (kJ mol^{-1}) while A_T is equilibrium binding constant equivalent to the maximum binding energy (L g^{-1}). T denotes temperature in kelvin whereas R gas constant *i.e.,* 8.314 × 10^{-3} kJ mol^{-1} K. A Temkin model graph can be plotted between qe and log Ce, (figure 12 c) values obtained are shown in table 3. The higher values of B_T signify high heat of adsorption.

Kinetics studies

The kinetic model regulates the rate of reaction. The kinetic study of MO adsorption onto FeNPs was calculated on 10 mg L^{-1} concentrations with pseudo I-order and pseudo II-order kinetic models.

The linear form of "Lagergren" pseudo I-order rate equation is as follows (Hu *et al.,* 2010):

$$\log(qe - qt) = \log qe - \frac{k_1}{2.303} t \quad \text{(Eq. 6)}$$

Where qt denotes the adsorbed MO concentration at time t (mg g^{-1}) whereas k_1 denotes rate constant (min^{-1}) for pseudo I order reaction. Value of Lagergren constant derived by plotting log (qe −qt) *vs* t Figure 13 a) are mentioned in table 4.

While the linear form for pseudo II-order can be expressed as (Hu *et al.,* 2010):

$$\frac{t}{q_t} = \frac{1}{(k_2 q_e^2)} + \left(\frac{1}{q_e}\right) t \quad \text{(Eq. 7)}$$

Where rate constant is denoted by k_2 (mg g^{-1} min^{-1}), after analyzing the experimental data for pseudo II-order kinetic model, the plot between t/qt *vs* t springs a straight line (Figure 13 b). Values for k_2 and R^2 are obtained from the plots are tabulated in table 4 with quite agreeable calculated adsorption capacity (q cal) with experimental data and higher R^2 value which ensures the present study of adsorption follow pseudo II-order. It further confirms that it is a type of chemisorption (Xu *et al.,* 2012):

Thermodynamics study of adsorption

For feasibility evaluation of the adsorption process of MO by FeNPs a thermodynamic study was performed. For calculating the thermodynamic parameters following equations were applied (Vimonses *et al*., 2009):

$$K_c = {}^{q_e}/_{C_e} \quad \text{(Eq. 8)}$$

$$\Delta G = \Delta H - T\,\Delta S \quad \text{(Eq. 9)}$$

$$ln\, K_c = \frac{\Delta S}{R} - \frac{\Delta H}{RT} \quad \text{(Eq. 10)}$$

Where, ΔG^o denotes Gibbs free energy change (kJ mol^{-1}) while the change in enthalpy by ΔH^o (kJ mol^{-1}), ΔS^o denoted by entropy change (J mol^{-1} K^{-1}), T is the temperature in kelvin, K_C is adsorption distribution coefficient. By plotting the graph in between ln K_C versus 1/T (figure 14), ΔH^o and ΔS^o were intended from its slope and intercept. After getting the values of ΔH^o and ΔS^o, value for ΔG^o was calculated as mentioned in table 5. The change in enthalpy determines the nature of (exothermic/endothermic) of the adsorption process. This further helps in differentiating the chemical and physical reaction of adsorption (Tseng *et al.,* 2010). For this adsorption study, negative value of ΔH^o confirms the reaction is exothermic in nature. However, at all temperatures studied ΔG^o values were negative, represents spontaneity of the adsorption process. Change in entropy (ΔS^o) predicts "magnitude of changes in the adsorbent surface", this due to the observed changes in the reversibility (Liu *et al*., 2010). The positive value for ΔS^o predicts the increased changeability.

CONCLUSION

As the studies prove, the organic compounds present in potential weed *D. inoxia* have a significant impact on the FeNPs stability and metal reduction. On the basis of equilibrium studies, a systematic investigation to determine the potential of FeNPs synthesized using aqueous leaf extract of *D. inoxia* for methyl orange adsorption has been performed. Characterization of FeNPs revealed they are amorphous in nature (as supported by XRD) having chain like structure with spherical morphology. The adsorption was maximally accessed at pH 2 because of interfacing of cation forming nature of FeNPs and the anionic MO azo dye. Langmuir model of adsorption and pseudo II-order fitted well to the MO adsorption by FeNPs. The adsorption process agreed reasonably well with the Langmuir isotherm and pseudo II-order, and R^2 = 0.99. Thermodynamics study proves the reaction is spontaneous and exothermic in nature. Better MO adsorption by FeNPs reaches in 75 minutes at equilibrium is desirable for other adsorption applications. The present adsorption study proposes the FeNPs to be applied as an efficient, substitute and low-cost adsorbent for textile wastewater treatment. It is a plant-based method that does not harm the environment, its structure and man. Hence, an environment friendly approach has been effectively applied.

CONFLICT OF INTEREST

No conflict of interest

ETHICAL CONDUCT

All co-authors have agreed to submit the manuscript to the journal. The findings have not been published elsewhere. This manuscript is not currently under consideration by

another journal.

REFERENCES

Ajmal A, Majeed I, Malik R N, Idriss H, Nadeem MA, (2014) Principles and mechanisms of photocatalytic dye degradation on TiO 2 based photocatalysts: a comparative overview. *RSC Adv* 4(70):37003-37026.

Ali I, Peng C, Ye T, Naz I, (2018) Sorption of cationic malachite green dye on phytogenic magnetic nanoparticles functionalized by 3-marcaptopropanic acid. *RSC Adv* 8(16):8878-8897.

Atul K, Pratibha C, Poonam V (2012). A comparative study on the treatment methods of textile dye effluents. *J Chem Pharm* 4(1) 763-771.

Ayawei N, Angaye SS, Wankasi D, Dikio ED (2015). Synthesis, characterization and application of Mg/Al layered double hydroxide for the degradation of congo red in aqueous solution. Open J Phys Chem5(03), 56.

Bagewadi ZK, Muddapur UM, Madiwal SS, Mulla SI, Khan A, (2019) Biochemical and enzyme inhibitory attributes of methanolic leaf extract of Datura inoxia Mill. *Environ Sustain* 2(1):75-87.

Beheshtkhoo N, Kouhbanani MAJ, Savardashtaki A, Amani AM, Taghizadeh S, (2018) Green synthesis of iron oxide nanoparticles by aqueous leaf extract of Daphne mezereum as a novel dye removing material. *Appl Phys A* 124(5):363.

Bhatia D, Sharma NR, Kanwar R, Singh J (2018). Physicochemical assessment of industrial textile effluents of Punjab (India). *App Water Sci* 8(3) 83.

Cao Y, Li X, (2014) Adsorption of graphene for the removal of inorganic pollutants in water purification: a review. *Adsorpt* 20(5-6):713-727.

Chen BY, Yen C, Chen W, *et al.,* (2009). Exploring threshold operation criteria of biostimulation for azo dye decolorization using immobi- lized cell systems. *Bioresour Technol* 100:5763–70.

Dąbrowski A, (2001) Adsorption—from theory to practice. Adv Colloid Interface Sci 93(1-3):135-224.

Daniel MC, Astruc D (2004). Gold nanoparticles: assembly, supramolecular chemistry, quantum-size-related properties, and applications toward biology, catalysis, and nanotechnology. *Chemical reviews* 104(1) 293-346.

de Médecine AN, (2009) Académie des Sciences, Académie des Technologies. In Réduirel'exposition aux ondes des antennes-relaisn'est pas justifiéscientifiquement. Rapport adopté le 15.

Debnath A, Deb K, Chattopadhyay KK, Saha B (2016). Methyl orange adsorption onto simple chemical route synthesized crystalline α-Fe2O3 nanoparticles: kinetic, equilibrium isotherm, and neural network modeling. *Desalination and Water Treatment* 57(29):13549-13560.

Deng H, Yang L, Tao G, Dai J, (2009) Preparation and characterization of activated carbon from cotton stalk by microwave assisted chemical activation—application in methylene blue adsorption from aqueous solution. *J Hazard Mater* 166(2-3):1514-1521.

do Socorro Vale M, Do Nascimento RF, Leitão RC, Santaella ST, (2016) Cr and Zn biosorption by Aspergillus niger. *Environ Earth Sci* 75(6):462.

Ebrahiminezhad A, Taghizadeh S, Ghasemi Y, Berenjian A (2018). Green synthesized nanoclusters of ultra-small zero valent iron nanoparticles as a novel dye removing material. *Sci Total Environ* 621:1527-1532.

Ebrahiminezhad A, Zare-Hoseinabadi A, Berenjian A, Ghasemi Y, (2017) Green synthesis and characterization of zero-valent iron nanoparticles using stinging nettle (Urtica dioica) leaf extract. *Green Process Synth* 6(5):469-475.

Erdem E, Çölgeçen G, Donat R, (2005) The removal of textile dyes by diatomite earth. *J Colloid Interface Sci* 282(2):314-319.

Fan J, Guo Y, Wang J, Fa M, (2009) Rapid decolorization of azo dye methyl orange in aqueous solution by nanoscale zerovalent iron particles. *J Hazard Mater* 166(2-3):904-910.

Feng J, Cerniglia CE, Chen H (2012) Toxicological significance of azo dye metabolism by human intestinal microbiota. Front BiosciElit 4:568.

Freyria FS, Esposito S, Armandi M, Deorsola F, Garrone E, Bonelli B (2017). Role of pH in the aqueous phase reactivity of zerovalent iron nanoparticles with acid orange 7, a model molecule of azo dyes. *J Nanomater*.

Ghaly AE, Ananthashankar R, Alhattab MVVR, Ramakrishnan VV (2014). Production, characterization and treatment of textile effluents: a critical review. *J Chem Eng Process Technol 5*(1):1-19.

Hu Z, Chen H, Ji F, Yuan S, (2010) Removal of Congo Red from aqueous solution by cattail root. *J Hazard Mat*er 173(1-3):292-297.

Javadian H, Taghavi M (2014) Application of novel Polypyrrole/thiol-functionalized zeolite Beta/MCM-41 type mesoporous silica nanocomposite for adsorption of Hg2+ from aqueous solution and industrial wastewater: Kinetic, isotherm and thermodynamic studies. *Appl Surf Sci* 289:487-494.

Kant R, (2011) Textile dyeing industry an environmental hazard. *Natural Sci* 4(1):22-26.

Kathiresan K, Manivannan S, Nabeel, MA, Dhivya B (2009). Studies on silver nanoparticles synthesized by a

marine fungus, Penicillium fellutanum isolated from coastal mangrove sediment. *Colloids Surf. B. Biointerfaces*, 71(1), 133-137.

Kaur J, Bansal S, Singhal S (2013). Photocatalytic degradation of methyl orange using ZnO nanopowders synthesized via thermal decomposition of oxalate precursor method. *Physica B: Condensed Matter*, 416, 33-38.

Kheshtzar R, Berenjian A, Taghizadeh SM, Ghasemi Y, Asad AG, Ebrahiminezhad A (2019). Optimization of reaction parameters for the green synthesis of zero valent iron nanoparticles using pine tree needles. *Green Process Synthes* 8(1), 846-855.

Kim SH, Choi PP (2017) Enhanced Congo red dye removal from aqueous solutions using iron nanoparticles: adsorption, kinetics, and equilibrium studies. *Dalt Trans* 46(44):15470-15479.

Kiran B, Kaushik A, (2008) Chromium binding capacity of Lyngbyaputealis exopolysaccharides. *Biochem Eng* J 38(1):47-54.

Krika F, Benlahbib OEF (2015) Removal of methyl orange from aqueous solution via adsorption on cork as a natural and low-coast adsorbent: equilibrium, kinetic and thermodynamic study of removal process. *Desalin Water Treat* 53(13):3711-3723.

Li XQ, Elliott DW, Zhang WX (2006) Zero-valent iron nanoparticles for abatement of environmental pollutants: materials and engineering aspects. *Crit Rev Solid State Mater Sci* 31(4):111-122.

Lin KF, Cheng HM, Hsu HC, Lin LJ, Hsieh WF, (2005) Band gap variation of size-controlled ZnO quantum dots synthesized by sol–gel method. *Chemic Physics Letters* 409(4-6):208-211.

Liou YH, Lo SL, Lin CJ, KuanWH, Weng SC, (2005) Chemical reduction of an unbuffered nitrate solution using catalyzed and uncatalyzed nanoscale iron particles. *J Hazard Mater* 127(1-3):102-110.

Liu QS, Zheng T, Wang P, Jiang JP, Li N, (2010) Adsorption isotherm, kinetic and mechanism studies of some substituted phenols on activated carbon fibers. *Chem Eng J* 157(2-3):348-356.

Luo P, Zhao Y, Zhang B, Liu J, Yang Y, Liu J, (2010) Study on the adsorption of Neutral Red from aqueous solution onto halloysite nanotubes. *Water Res* 44(5):1489-1497.

Machado S, Pinto SL, Grosso JP, Nouws HPA, Albergaria JT, Delerue-Matos C, (2013) Green production of zero-valent iron nanoparticles using tree leaf extracts. *Sci Total Environ* 445:1-8.

Mahdavi M, Namvar F, Ahmad MB, Mohamad R, (2013) Green biosynthesis and characterization of magnetic iron oxide (Fe3O4) nanoparticles using seaweed (Sargassum muticum) aqueous extract. *Molecules* 18(5):5954-5964.

Massoud A, Mahmoud HH (2017). Evaluation of hybrid polymeric resin containing nanoparticles of iron oxide for selective separation of In (III) from Ga (III). J InorgOrganometPolym Mater 27(6):1806-1815.

Mathur N, Bhatnagar P, Sharma P (2012). Review of the mutagenicity of textile dye products. *Univers* J Environ 2(2).

Mittal AK, Chisti Y, Banerjee UC (2013) Synthesis of metallic nanoparticles using plant extracts. *Biotechnol Adv* 31(2):346-356.

Mondal, N. K. (2015). Green Synthesis of Silver nanoparticle and its application for removal of dye from aqueous solution. *Int J Chem* 1(1):1-12.

Njagi EC, Huang H, Stafford L, Genuino H, Galindo HM, Collins JB, Suib SL, (2011) Biosynthesis of iron and silver nanoparticles at room temperature using aqueous sorghum bran extracts. *Langmuir* 27(1):264-271.

NTP U (1992). Specification for the Conduct of Studies to Evaluate the Toxic and Carcinogenic Potential of Chemical, Biological and Physical Agents in Laboratory Animals for the National Toxicology Program (NTP), Research Triangle Park, NC. Research Triangle Park, NC: US National Toxicology Program.

Pattanayak M, Nayak PL (2013b). Ecofriendly green synthesis of iron nanoparticles from various plants and spices extract. ICHNOS, 3(1), 68-78.

Pattanayak M, Nayak PL, (2013a) Green synthesis and characterization of zero valent iron nanoparticles from the leaf extract of Azadirachta indica (Neem). *World J Nano Sci Tech* 2(1):06-09.

Pielesz A, Baranowska I, Rybak A, Włochowicz A. (2002). Detection and determination of aromatic amines as products of reductive splitting from selected azo dyes. *Ecotoxicol Environ Saf*, 53, 42–7.

Prasad SS, Aikat K. (2014). Study of bio-degradation and bio-decolourization of azo dye by Enterobacter sp. SXCR. *Environ Technol* 35:956–65.

Raman CD, Kanmani S (2016). Textile dye degradation using nano zero valent iron: a review. *J Environ Manage177*:341-355.

Saha B, Das S, Saikia J, Das G (2011) Preferential and enhanced adsorption of different dyes on iron oxide nanoparticles: a comparative study. *J Phys Chem C* 115(16):8024-8033.

Saif, S., Tahir, A., & Chen, Y. (2016). Green synthesis of iron nanoparticles and their environmental applications and implications. *Nanomaterials* 6(11):209.

Sajab MS, Chia CH, Zakaria S, Jani SM, Ayob MK, Chee KL, Chiu WS, (2011) Citric acid modified kenaf core

fibres for removal of methylene blue from aqueous solution. *Bioresour Technol* 102(15):7237-7243.

Sebastian A, Nangia A, Prasad MNV, (2018) Green Synthesis of Iron Nanoparticles from Selected Plant Materials of Peninsular India. *Proceedings of the National Academy of Sciences, India Section A: Physical Sciences* 88(2):195-203.

Shahwan, T. Sirriah, S. A. Nairat, M. Boyacı, E. Eroğlu, A. E. Scott, T. B. and Hallam, K. R. 2011. Green synthesis of iron nanoparticles and their application as a Fenton-like catalyst for the degradation of aqueous cationic and anionic dyes. *Chemical Engineering Journal*, 172(1):258-266.

Silva, AKA, Espinosa A, Kolosnjaj-Tabi J, Wilhelm C, Gazeau F (2016). Medical applications of iron oxide nanoparticles. Iron Oxides: *From Nature to Applications*.

Sundararajan M, Thomas PA, Babyshalini K, Geraldine P, (2017) Identification of phytoconstituents and in-vitro evaluation of the putative anticataractogenic effect of an ethanolic root extract of Leucas aspera. *Biomedicine & Pharmacotherapy* 85:87-101.

Tauber MM, Guebitz GM, Rehorek A (2005). Degradation of azo dyes by laccase and ultrasound treatment. Appl Environ Microbiol, 71, 2600–7.

Tseng RL, Wu KT, Wu FC, Juang RS, (2010) Kinetic studies on the adsorption of phenol, 4-chlorophenol, and 2, 4-dichlorophenol from water using activated carbons. *J Environ Manage* 91(11):2208-2214.

Vimonses V, Lei S, Jin B, Chow CW, Saint C, (2009) Adsorption of congo red by three Australian kaolins. *Appl Clay Sci* 43(3-4):465-472.

Walker JM, Zaleski JM (2016). A simple route to diverse noble metal-decorated iron oxide nanoparticles for catalysis. *Nanoscal*e 8(3):1535-1544.

Wang Y, Zhao H, Zhao G (2015). Iron-copper bimetallic nanoparticles embedded within ordered mesoporous carbon as effective and stable heterogeneous Fenton catalyst for the degradation of organic contaminants. *Applied Catalysis B: Environmental*, 164:396-406.

Weber TW, Chakravorti RK, (1974) Pore and solid diffusion models for fixed-bed adsorbers. *AIChE Journal*, 20(2):228-238.

Xin X, Wei Q, Yang J, Yan L, Feng R, Chen G, Li H, (2012) Highly efficient removal of heavy metal ions by amine-functionalized mesoporous Fe3O4 nanoparticles. *Chem Eng J* 184:132-140.

Yao L, Zhang L, Wang R, Chou S, Dong Z, (2016) A new integrated approach for dye removal from wastewater by polyoxometalates functionalized membranes. *J Hazard Mater* 301:462-470.

Youssef NA, Shaban SA, Ibrahim FA, Mahmoud AS (2016). Degradation of methyl orange using Fenton catalytic reaction. *Egyptian Journal of Petroleum*, *25*(3):317-321.

Yu WJ, Liu C, Zhang L, Hou PX, Li F, Zhang B, Cheng HM (2016). Synthesis and electrochemical lithium storage behavior of carbon nanotubes filled with iron sulfide nanoparticles. Advanced Science 3(10):1600113.